AGU PUBLICATIONS

Geophysical Research Letters

RESEARCH LETTER
10.1002/2014GL059322

Special Section:
Early Results from the Van Allen Probes

The role of ring current particle injections: Global simulations and Van Allen Probes observations during 17 March 2013 storm

Yiqun Yu[1], Vania Jordanova[1], Dan Welling[2], Brian Larsen[1], Seth G. Claudepierre[3], and Craig Kletzing[4]

[1]Los Alamos National Laboratory, Los Alamos, New Mexico, USA, [2]Department of Atmospheric, Oceanic, and Space Sciences, University of Michigan, Ann Arbor, Michigan, USA, [3]The Aerospace Corporation, Los Angeles, California, USA, [4]Department of Physics and Astronomy, Iowa University, Iowa City, Iowa, USA

Key Points:
- New capability for studying substorm-associated depolarization and injections
- Advanced from previous technique that used artificial electromagnetic pulses
- The model well produces injections and electron fluxes observed from Van Allen Probes

Correspondence to:
Y. Yu,
yiqun@lanl.gov

Citation:
Yu, Y., V. Jordanova, D. Welling, B. Larsen, S. G. Claudepierre, and C. Kletzing (2014), The role of ring current particle injections: Global simulations and Van Allen Probes observations during 17 March 2013 storm, *Geophys. Res. Lett.*, *41*, 1126–1132, doi:10.1002/2014GL059322.

Received 16 JAN 2014
Accepted 30 JAN 2014
Accepted article online 4 FEB 2014
Published online 22 FEB 2014

Abstract We simulate substorm injections observed by the Van Allen Probes during the 17 March 2013 storm using a self-consistent coupling between the ring current model RAM-SCB and the global MHD model BATS-R-US. This is a significant advancement compared to previous studies that used artificially imposed electromagnetic field pulses to mimic substorm dipolarization and associated inductive electric field. Several substorm dipolarizations and injections are reproduced in the MHD model, in agreement with the timing of shape changes in the *AE*/*AL* index. The associated inductive electric field transports plasma sheet plasma to geostationary altitudes, providing the boundary plasma source to the ring current model. It is found that impulsive plasma sheet injections, together with a large-scale convection electric field, are necessary to develop a strong ring current. Comparisons with Van Allen Probes observations show that our model reasonably well captures dispersed electron injections and the global *Dst* index.

1. Introduction

The outer electron radiation belt is substantially variable during geomagnetic disturbed times and its enhancement can create potential hazards to spaceborne electronics, disrupting communications, power systems, and navigations [e.g., *Baker et al.*, 1994]. Understanding the physical processes that account for the variability of the electron radiation belts is therefore of great interest and is the leading objective of the Van Allen Probes Mission [*Mauk et al.*, 2012]. Specifically, the study of ring current (energy from ~ 1 keV to hundreds of keV) dynamics is significant because the ring current not only provides the crucial electron seed population for the radiation belts but also carries the most plasma energy density of the inner magnetosphere and determines the global distribution of magnetic fields that affect the motion of radiation belt particles. Numerical models have been developed to investigate ring current dynamics and its various geomagnetic effects [e.g., *Chen et al.*, 1994; *Jordanova et al.*, 1994; *Toffoletto et al.*, 2003]. Recently, significant effort has been put into developing a ring current model with full physical coupling between the plasma and fields, that is, electromagnetic fields self-consistently computed with particles [e.g., *Fok et al.*, 2001; *Lemon et al.*, 2004; *Zaharia et al.*, 2006]. The ring current not only changes the global magnetic configuration but also affects current systems that link to the ionosphere and the electric field. The subsequent changes in the magnetic and electric fields can be large enough to redistribute ring current particles. This therefore suggests the need for a self-consistent approach in the model to include the feedback between the fields and plasma.

Substorms generally involve electron injections of energy up to a few hundred keV from the magnetotail toward the inner magnetosphere, providing important seed populations for ring current and radiation belt as well as free energy for the excitation of various plasma waves [e.g., *Meredith et al.*, 2003] to interact with energetic particles. Substorms are associated with magnetic field stretching and subsequent dipolarization, which induces electric fields that transport tail plasma sheet particles toward the Earth. Previous models simulate particle injections by superposing artificial, spatially localized electromagnetic pulses, with prescribed propagation speed and azimuthal extent, over the background magnetic field to mimic the magnetotail dipolarization and associated induced electric field [e.g., *Li et al.*, 1998; *Sarris et al.*, 2002; *Zaharia et al.*, 2004; *Liu et al.*, 2009; *Ganushkina et al.*, 2013]. Although these injection models can reasonably capture electron injections observed at geosynchronous orbit (GEO), the use

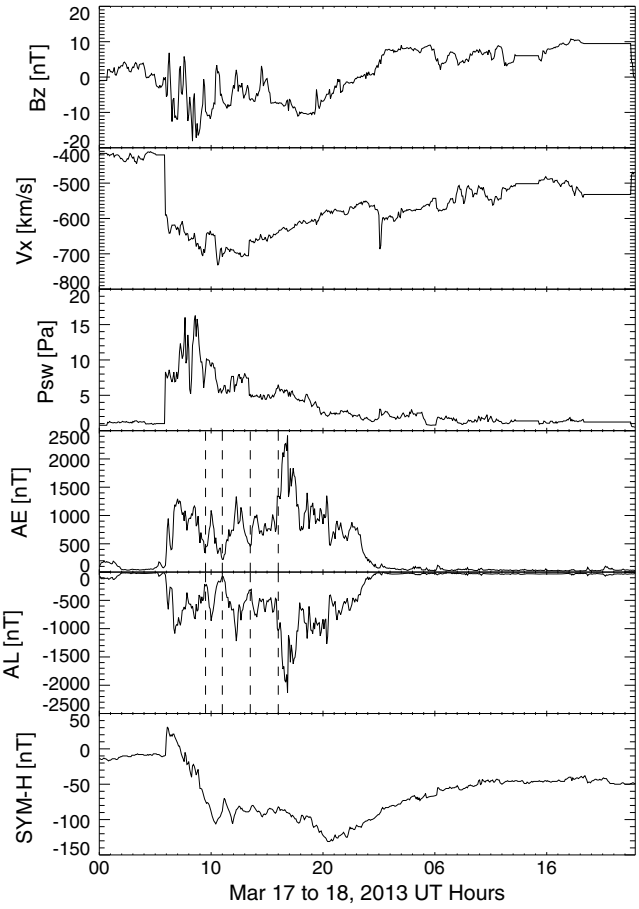

Figure 1. Overview of the magnetic storm on 17 and 18 March 2013. The solar wind data, interplanetary magnetic field, *AE*, *AL*, and *SYM-H* indices are obtained from OMNIWeb. The vertical lines mark the time when *AE*/*AL* index begins to sharply increase/decrease.

of postulated electromagnetic pulses leaves the system inconsistent because it omits the feedback of inner magnetospheric dynamics on the global-scale electromagnetic fields that initiate injections. This study presents a significant advancement in ring current simulations, employing a self-consistent modeling of plasma and electromagnetic fields for substorm injections and testing the model capabilities in reproducing recent observations from the Van Allen Probes during a magnetic storm event. It is found that the model is capable of capturing substorm-associated dipolarizations that provide impulsive abundant plasma source to the ring current. A large-scale convection electric field is also necessary to transport the plasma sheet particles from geosynchronous altitudes inward to develop an intense ring current. The model also reasonably reproduces dispersed/dispersionless electron flux injections observed by the Van Allen Probes.

2. Model Description

The ring current dynamics is simulated with the RAM-SCB model [*Jordanova et al.*, 2010; *Zaharia et al.*, 2006] that couples two codes: (1) the kinetic Ring current-Atmosphere Interactions model (RAM), which solves the bounce-averaged particle distribution for major ring current species and (2) a 3-D Euler-potential-based plasma equilibrium magnetic field code. The RAM solves the phase space distribution for H^+, He^+, O^+, and electrons in the magnetic equatorial plane as a function of radial distance (2 R_E to 6.5 R_E), all magnetic local times, energy (~100 eV to ~400 keV), and pitch angle (0° to 90°). The loss processes for the ring current ions include charge exchange with geocoronal hydrogen and collisions with the dense atmosphere, while losses due to atmosphere collisions and wave-particle interactions are considered for the electrons (see details in *Jordanova et al.* [2012]). The plasma pressure produced by the ring current distribution is used in the 3-D equilibrium code to calculate the force balanced magnetic field, which is then used to propagate the phase space distribution function.

The RAM-SCB is, for the first time, two-way coupled with the MHD code BATS-R-US, advanced from the previous one-way coupling [*Zaharia et al.*, 2010]. That is, instead of taking the output from the MHD code without feeding back the ring current pressure to the MHD code, this study steps toward an initial two-way coupling, establishing the self consistency in the electric field for RAM-SCB and also allowing for the modeling of a realistic global magnetic field configuration. The MHD code provides plasma boundary condition for RAM-SCB at geosynchronous orbit, with an assumption of an isotropic kappa distribution (κ=3) with density and characteristic temperature taken from the MHD code. In return, the MHD pressure in the inner magnetosphere region is modified by the RAM-SCB pressure, which subsequently alters the global magnetospheric configuration and current systems. The field-aligned currents are passed to the ionospheric potential solver [*Ridley et al.*, 2004] to determine the electric potential, which is used to provide the convection electric field for the drift of ring current particles within the RAM-SCB model. The ring current model is thus driven by

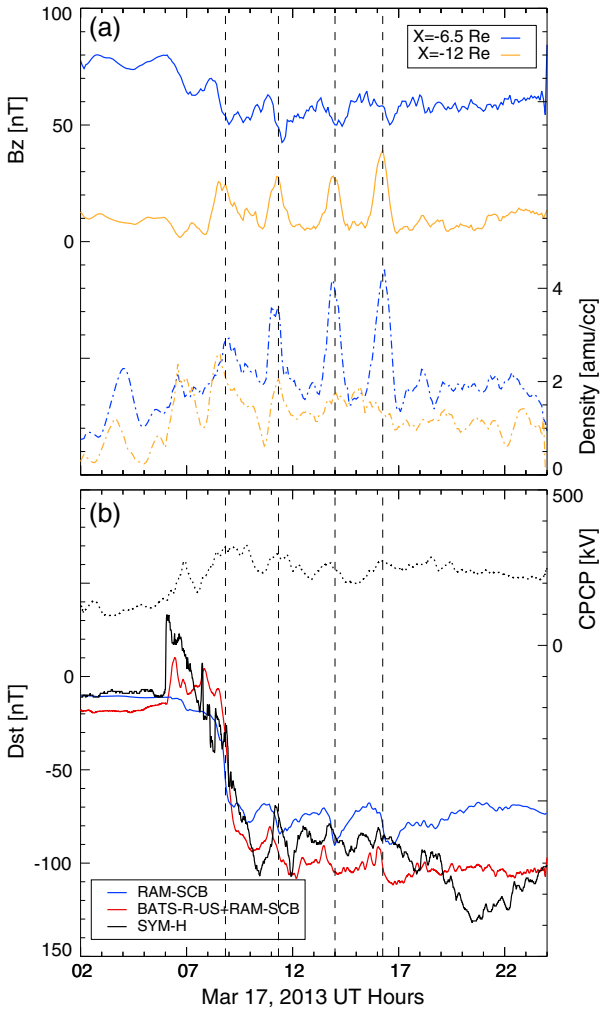

Figure 2. (a) Magnetic field B_z (solid lines) and plasma density (dashed lines) at two different equatorial midnight locations: −6.5 R_E (blue) and −12.0 R_E (orange), obtained from the MHD output. The plasma density at −6.5 R_E provides the plasma boundary condition to the RAM-SCB model after assuming a kappa distribution with its characteristic temperature taken from the MHD. (b) The observed *SYM-H* index (black) and *Dst* index calculated from the ring current model RAM-SCB (blue) and the global MHD model BATS-R-US coupled with RAM-SCB (red). The dashed line is the ionospheric cross polar cap potential (CPCP) index. Vertical dashed lines indicate the time of tail injections in the model.

a self-consistent electric field in addition to its already existing self-consistently calculated magnetic field.

In the MHD code, the ring current pressure feedback results in a more stretched, realistic global magnetospheric configuration and thus allows for the modeling of realistic substorm-associated dipolarization and injection. Magnetotail plasma is injected earthward from the tail reconnection site, in virtue of the inductive electric field from the time-varying magnetic field. Unlike previous studies in which substorm injections are modeled via artificially imposed electric field pulses, this study treats the electromagnetic fields, associated with substorm injections, self consistently with ring current dynamics.

3. Results

With the above two-way coupling setup, we simulate the 17 March 2013 storm event, using the observed upstream solar wind conditions shifted to the outer boundary of the MHD code (i.e., 32 R_E). Figure 1 displays the upstream solar wind condition near the bow shock, and the *AE*/*AL* and *SYM-H* indices. Approximately at 6:00 UT on 17 March, a coronal mass ejection (CME) driven shock arrived at the magnetosphere, with sudden enhancement in the solar wind dynamic pressure and southward turning of B_z. The *SYM-H* index, a proxy of the ring current intensity, reaches −100 nT at 10:00 UT; a second dip occurs around 20:00 UT reaching down to −140 nT before it starts recovering. During the storm main phase substantial substorm activities are observed (see the *AE*/*AL* index).

Figure 2a shows magnetic field and plasma density at two different locations on the midnight equator from the MHD model. Periodic injections are produced, characterized by magnetic field dipolarizations and enhanced plasma density near −6.5 R_E around 09:00, 11:20, 14:00, and 16:15 UT respectively. The dipolarization signatures at 6.5 R_E are not as prominent as in the midtail but at each instance (vertical lines) B_z is abruptly increased, though with a small amplitude. The enhanced plasma density is injected from the magnetotail toward the Earth by the large electric field induced from the rapidly varying magnetic field. The above injections resemble the real substorm activities, since the *AE* (*AL*) index begins to sharply increase (decrease) at 09:30, 11:00, 13:30, and 16:00 UT (Figure 1), approximately aligned with the modeled dipolarizations and injections, and these sharp changes in the *AE*/*AL* index occur almost simultaneously with substorm onset [*Weygand et al.*, 2008]. The large increase (decrease) in *AE* (*AL*) index between 18:00 and 20:00 UT suggests further substorm injections, which are however missed in the model.

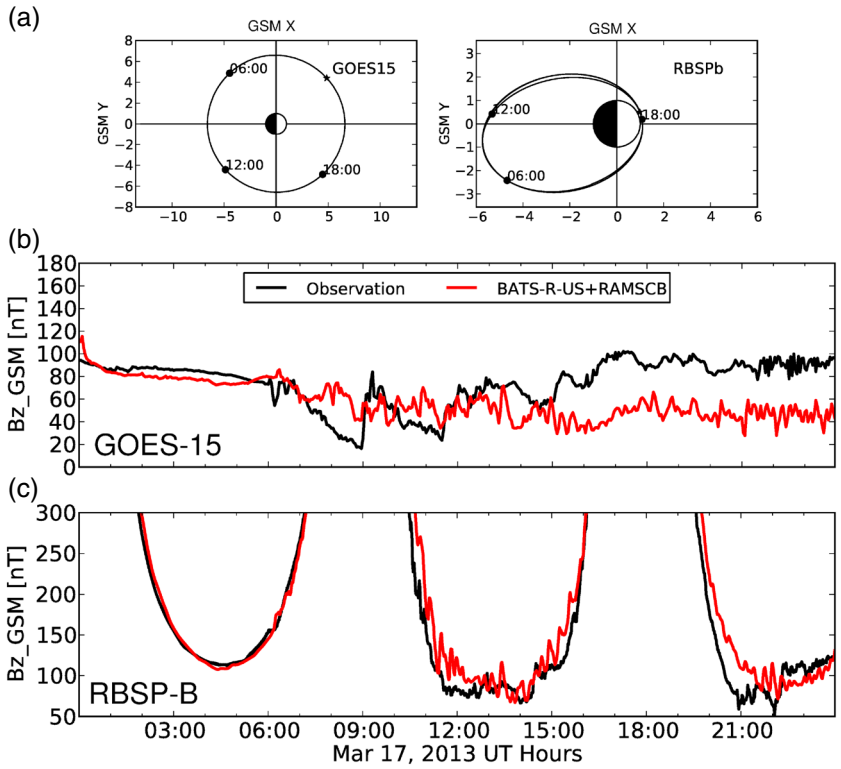

Figure 3. (a) The orbits of GOES-15 and Van Allen Probes-B in the GSM *XY* plane. (b) Comparison of in situ magnetic field (B_z component) along GOES-15 (black) and simulation (red). (c) Comparison of in situ magnetic field (B_z component) along Van Allen Probes-B (black) and simulation (red).

The above injections provide large plasma source to the RAM-SCB model through the nightside boundary at 6.5 R_E, and the enhanced convection electric field, represented by the global cross polar cap potential (CPCP) index (Figure 2b, dashed line), serves as an important driver for convecting the boundary plasma earthward, forming a strong ring current. The *Dst* index calculated with the Dessler-Parker-Sckopke [*Sckopke*, 1966] relation based on ring current energy content within 6.5 R_E (Figure 2b, blue line) shows periodic enhancement, highly correlated with those injection instances (vertical lines), suggesting that tail plasma injections are an important source for the ring current intensification. The *Dst* index, calculated from Biot-Savart integral law in the global MHD model (Figure 2b, red line), is further enhanced when current systems other than the ring current (such as tail current) are taken into account and agrees well with the observed *SYM-H* index.

Figure 3 shows comparisons of the magnetic field *Z* component with measurements from GOES-15 and Van Allen Probe-B/Electric and Magnetic Field Instrument Suite and Integrated Science (EMFISIS) [*Kletzing et al.*, 2013]. With a two-way coupling between RAM-SCB and BATS-R-US, the MHD model reproduces very well the magnetic field measured by EMFISIS inside GEO. However, from the comparison on GOES-15, the *Z* component magnetic field in the dayside magnetosphere after 15:00 UT is underestimated in the model and the signatures of the dipolarization at nightside are not well reproduced (e.g., 09:00 UT near midnight and 11:30 UT near 02 MLT). For the latter situation, although the model does show dipolarization signatures near midmagnetotail (see Figure 2, at 12 R_E), the signature near GEO (6.5 R_E) significantly diminishes, suggesting that in the model the injection from the tail does not propagate deep down to GEO. On the other hand, the underestimation of the dayside magnetic field indicates a less compressed dayside cavity in the model.

Figure 4 shows ring current electron flux compared to flux observed from Energetic Particle Composition and Thermal Plasma Suite (ECT)/magnetic electron ion spectrometer (MagEIS) instrument [*Blake et al.*, 2013] onboard Van Allen Probes-B. Figures 4a and 4b display the electron flux spectrogram from the ECT/MagEIS measurements and model output, while Figures 4c and 4d are electron fluxes at several different energy levels, extracted from Figures 4a and 4b, respectively. The ring current model, taking boundary conditions from the MHD model, captures reasonably well the major dynamic features in the ring current electron

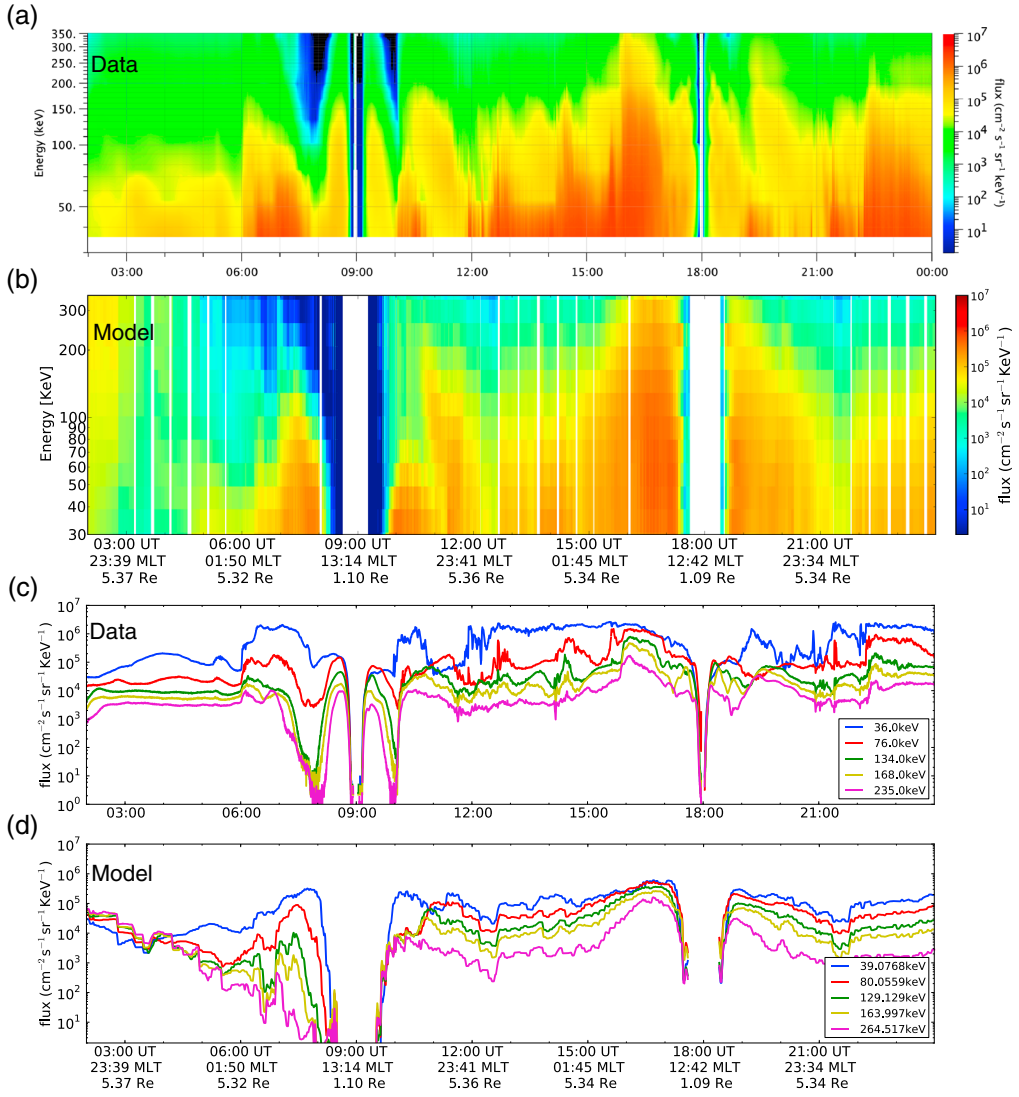

Figure 4. (a) Spin-averaged electron flux spectrogram observed by the ECT/MagEIS instruments aboard Van Allen Probe-B. *Y* axis covers energy range from 30 to 350 keV. The blank region below around 40 keV is because it is below the instrument limit. (b) The simulated flux spectrogram from RAM-SCB coupled with BATS-R-US, averaged over pitch angle, in the same format. The white strips in the simulated flux spectrogram are gaps in the model output when the satellite is outside the computational domain. (c) The electron fluxes extracted from Figure 4a at different energy levels. (d) The electron fluxes extracted from Figure 4b at different energy levels.

flux, including the rapid increase after the shock impinging on the magnetosphere around 6:00 UT, the energy-dispersed injection from 11:00 to 12:00 UT near the midnight, and several other weak dispersionless injections during the storm main phase. By comparing Figures 4c and 4d after 12:00 UT, it is found that while the high-energy flux is well reproduced by the model, flux at low energies near 30 keV is about 1 order of magnitude lower than the observed fluxes in the main phase. After 18:00 UT, the modeled electron flux is not as dynamic as in the measurement due to the absence of notable tail activities in the MHD model and thereby the absence of large impulsive plasma source into the ring current model. The large flux seen at the beginning of the simulation is attributed to the initial condition in the model which needs a few hours to be completely replaced by new plasma source transported from the nightside.

4. Discussion and Conclusion

This study investigated substorm plasma injections from the plasma sheet into the ring current, using a self-consistent treatment between the electromagnetic fields and ring current dynamics. Previous studies

used artificial electromagnetic pulses to represent smaller-scale fields associated with substorms to transport plasma sheet particles toward the Earth. Such a method is usually limited by the pulse model itself, because the free parameters in the model first requires fitting with observations before they are adapted in the pulse model. These parameters include the pulse propagating velocity, azimuthal extent, impact location, etc. All these parameters should not be fixed but rather time dependent and influenced by the ring current dynamics. Therefore, a self-consistent modeling of the ring current dynamics and the substorm electromagnetic fields is necessary. This study used a two-way coupling between a ring current model and a global MHD model. It allowed for the self-consistent modeling of substorm-associated dipolarization and inductive electric field and the subsequent transport of impulsive plasma sheet source to the ring current, which in return modifies the global magnetospheric configuration.

The global MHD model, with the ring current pressure feedback, generated several substorm-associated dipolarizations and injections during the storm main phase, in good agreement with the timing of substorm onset represented by sharp increase (decrease) in the observed *AE* (*AL*) index. These injections provided important plasma source from the plasma sheet to the ring current, creating a strong ring current, with the coexisting large convection electric field. When injections (i.e., around 20:00 UT) are not captured by the model, it results in a weaker ring current, which suggests that impulsive plasma sheet source transported through the substorm-associated dipolarization electric field is necessary to intensify the ring current. The elevated large-scale convection electric field alone (the CPCP index remains about 200 kV around 20:00 UT) is not sufficient to develop the large dip in the observed *Dst* index, implying that a supply of plasma sheet source from the tail is needed.

This first ring current modeling result using the two-way coupling method showed that the model can generally capture the observed ring current dynamics, including a sudden increase of flux after the shock arrival, dispersed/dispersionless electron injections, and the global proxy of ring current energy—*Dst* index. The model reproduced well the high-energy fluxes, however, underestimated the electron fluxes at low energies (around 30 keV) by 1 order of magnitude. One possible explanation lies in the boundary condition. A kappa distribution was assumed for the ring current particle flux at the nightside boundary 6.5 R_E, based on the MHD density and temperature. Such a distribution is quasi-Maxwellian at low and thermal energies with a gradual falling shape, which however deviates from the non-Maxwellian spectra at GEO [*Jordanova et al.*, 2010] that usually have larger fluxes at lower energies. In addition, although the model clearly produced periodic dipolarization near 12 R_E in the tail, the dipolarization signature at geostationary orbit was diminished compared to the observation from GOES-15. This may suggest that the tail reconnection site was too far in the model or that the near-Earth braking force was too large. The effect of boundary condition and the tail reconnection will be subject of our future investigation.

Acknowledgments

This work was supported by JHU/APL contracts 967399 and 921647, under NASA's primer contract NAS5-01072. The analysis at LANL was supported by EMFISIS subaward NNG13PJ05I and NSF grant 1203460. We thank the OMNIWeb from NASA Goddard Space Flight Center for providing the solar wind observation data and the Kyoto, Japan, World Data Center System for providing the *AE* index.

The Editor thanks two anonymous reviewers for their assistance in evaluating this paper.

References

Baker, D. N., S. Kanekal, J. B. Blake, B. Klecker, and G. Rostoker (1994), Satellite anomalies linked to electron increase in the magnetosphere, *Eos Trans. AGU*, *75*, 401–405, doi:10.1029/94EO01038.

Blake, J., et al. (2013), The magnetic electron ion spectrometer (MagEIS) instruments aboard the radiation belt storm probes (RBSP) spacecraft, *Space Sci. Rev.*, *179*, 383–421, doi:10.1007/s11214-013-9991-8.

Chen, M. W., L. R. Lyons, and M. Schulz (1994), Simulations of phase space distributions of storm time proton ring current, *J. Geophys. Res.*, *99*, 5745–5759, doi:10.1029/93JA02771.

Fok, M.-C., R. A. Wolf, R. W. Spiro, and T. E. Moore (2001), Comprehensive computational model of Earth's ring current, *J. Geophys. Res.*, *106*, 8417–8424, doi:10.1029/2000JA000235.

Ganushkina, N. Y., O. A. Amariutei, Y. Y. Shprits, and M. W. Liemohn (2013), Transport of the plasma sheet electrons to the geostationary distances, *J. Geophys. Res. Space Physics*, *118*(1), 82–98, doi:10.1029/2012JA017923.

Jordanova, V. K., J. U. Kozyra, G. V. Khazanov, A. F. Nagy, C. E. Rasmussen, and M.-C. Fok (1994), A bounce-averaged kinetic model of the ring current ion population, *Geophys. Res. Lett.*, *21*, 2785–2788, doi:10.1029/94GL02695.

Jordanova, V. K., S. Zaharia, and D. T. Welling (2010), Comparative study of ring current development using empirical, dipolar, and self-consistent magnetic field simulations, *J. Geophys. Res.*, *115*, A00J11, doi:10.1029/2010JA015671.

Jordanova, V. K., D. T. Welling, S. G. Zaharia, L. Chen, and R. M. Thorne (2012), Modeling ring current ion and electron dynamics and plasma instabilities during a high-speed stream driven storm, *J. Geophys. Res.*, *117*(A9), A00L08, doi:10.1029/2011JA017433.

Kletzing, C., et al. (2013), The Electric and Magnetic Field Instrument Suite and Integrated Science (EMFISIS) on RBSP, *Space Sci. Rev.*, *179*, 127–181, doi:10.1007/s11214-013-9993-6.

Lemon, C., R. A. Wolf, T. W. Hill, S. Sazykin, R. W. Spiro, F. R. Toffoletto, J. Birn, and M. Hesse (2004), Magnetic storm ring current injection modeled with the Rice Convection Model and a self-consistent magnetic field, *Geophys. Res. Lett.*, *31*, L21801, doi:10.1029/2004GL020914.

Li, X., D. N. Baker, M. Temerin, G. D. Reeves, and R. D. Belian (1998), Simulation of dispersionless injections and drift echoes of energetic electrons associated with substorms, *Geophys. Res. Lett.*, *25*(20), 3763–3766, doi:10.1029/1998GL900001.

Liu, W. L., et al. (2009), Observation and modeling of the injection observed by THEMIS and LANL satellites during the 23 March 2007 substorm event, *J. Geophys. Res.*, *114*(A1), A00C18, doi:10.1029/2008JA013498.

Mauk, B. H., N. J. Fox, S. G. Kanekal, R. L. Kessel, D. G. Sibeck, and A. Ukhorskiy (2012), Science objectives and rationale for the Radiation Belt Storm Probes Mission, *Space Sci. Rev.*, *179*, 3–27, doi:10.1007/s11214-012-9908-y.

Meredith, N. P., R. M. Thorne, R. B. Horne, D. Summers, B. J. Fraser, and R. R. Anderson (2003), Statistical analysis of relativistic electron energies for cyclotron resonance with EMIC waves observed on CRRES, *J. Geophys. Res.*, *108*(A6), 1250, doi:10.1029/2002JA009700.

Ridley, A., T. Gombosi, and D. Dezeeuw (2004), Ionospheric control of the magnetosphere: Conductance, *Ann. Geophys.*, *22*, 567–584, doi:10.5194/angeo-22-567-2004.

Sarris, T. E., X. Li, N. Tsaggas, and N. Paschalidis (2002), Modeling energetic particle injections in dynamic pulse fields with varying propagation speeds, *107*, *A3*, SMP 1-1–SMP 1-10, doi:10.1029/2001JA900166.

Sckopke, N. (1966), A General relation between the energy of trapped particles and the disturbance field near the Earth, *J. Geophys. Res.*, *71*, 3125–3130, doi:10.1029/JZ071i013p03125.

Toffoletto, F., S. Sazykin, R. Spiro, and R. Wolf (2003), Inner magnetospheric modeling with the Rice Convection Model, *Space Sci. Rev.*, *107*, 175–196, doi:10.1023/A:1025532008047.

Weygand, J. M., R. L. McPherron, K. Kauristie, H. U. Frey, and T.-S. Hsu (2008), Relation of auroral substorm onset to local AL index and dispersionless particle injections, *J. Atmos. Sol. Terr. Phys.*, *70*, 2336–2345, doi:10.1016/j.jastp.2008.09.030.

Zaharia, S., C. Cheng, and K. Maezawa (2004), 3-D force-balanced magnetospheric configurations, *Ann. Geophys.*, *22*, 251–265, doi:10.5194/angeo-22-251-2004.

Zaharia, S., V. K. Jordanova, M. F. Thomsen, and G. D. Reeves (2006), Self-consistent modeling of magnetic fields and plasmas in the inner magnetosphere: Application to a geomagnetic storm, *J. Geophys. Res.*, *111*, A11S14, doi:10.1029/2006JA011619.

Zaharia, S., V. K. Jordanova, D. Welling, and G. Tóth (2010), Self-consistent inner magnetosphere simulation driven by a global MHD model, *J. Geophys. Res.*, *115*, A12228, doi:10.1029/2010JA015915.